Eurographics Workshop on Visual Computing for Biology and Medicine (2015)
K. Bühler, L. Linsen, and N. W. John (Editors)

A Two-Level Cascade Classification Algorithm for Real-Time Bifurcation Detection in CTA Images of Blood Vessels

A. A. Novikov, M. Wimmer, D. Major, and K. Bühler

VRVis Center for Virtual Reality and Visualization, Vienna, Austria

Abstract

We introduce a cascade classification algorithm for bifurcation detection in Computed Tomography Angiography (CTA) scans of blood vessels. The proposed algorithm analyzes the vessel surrounding by a trained classifier first, followed by an accurate segmentation of the vessel outer wall by Morphological Active Contour Without Edges and finally extracts the boundary features of the segmented object and classifies its shape by Approximate K-nearest Neighbour classifier. The algorithm shows encouraging and competitive results for blood vessels from various parts of a human body including head, neck and legs.

Categories and Subject Descriptors (according to ACM CCS): I.4.8 [Image Processing and Computer Vision]: Scene Analysis—Object recognition

1. Introduction

Vascular diseases such as atherosclerosis and stenosis often affect human vessels and can lead to serious problems, including heart attack, stroke, or even death. To timely diagnose and treat such diseases, medical imaging techniques are widely used with CTA being particularly suitable for producing detailed images of blood vessels and tissues in various parts of the body. Image processing and machine learning techniques can help to accelerate and facilitate daily routines of physicians. Robust segmentation and labeling of vessels is important for accurate calcification, plaque and lumen segmentation. Consequently, this can help to better identify symptoms and diagnose many dangerous vascular diseases.

However, to represent the complete vessel tree morphometry, precise vessel segmentation is not sufficient and detection of vessel landmarks such as bifurcations is needed. A vessel bifurcation is the point at which division into two smaller vessels occurs (see Figure 1). An accurate algorithm for bifurcation detection could be of use for postprocessing of existing tracked vessels or can be as well a part of a larger vessel tracking or labeling system. In this work we propose an algorithm which could be fully or partially used for such applications.

Related work There has been a large amount of studies focused on lumen and vessel outer wall segmentation algorithms however only few of them target the bifurcation detection problem. This problem still remains a major challenge.

Alberti et al. [ABG*12] presented a fully automatic method for detecting bifurcations in intravascular ultrasound sequences. The algorithm proceeds in two steps: first, angular sector classification is applied to image sequences. Second, the results were refined by using contextual information for a multiscale stacked sequential learning scheme. Though results are great, the designed features are very specific for ultrasound sequences and therefore not easy to adjust for other modalities.

A bifurcation filter based on modeling bifurcations in scale space and combined with eigenvalue analysis was proposed by Baboiu et al. [BH12]. The algorithm was substantially evaluated on synthetically generated 2D bifurcations as well as on medical data on large retinal angiograms with each containing several hundred bifurcations. No quantitative results for 3D volumes were reported.

Beck et al. [BBBD10] detected and validated vessel bifurcation landmarks by using Fast Marching and anatomical information from a knowledge database. The algorithm was tested on datasets with carotids only. Success rates of 74.47 % for right and 78.72 % for left carotid bifurcations were reported. Though results are good on the carotids, it is not

DOI: 10.2312/vcbm.20151216

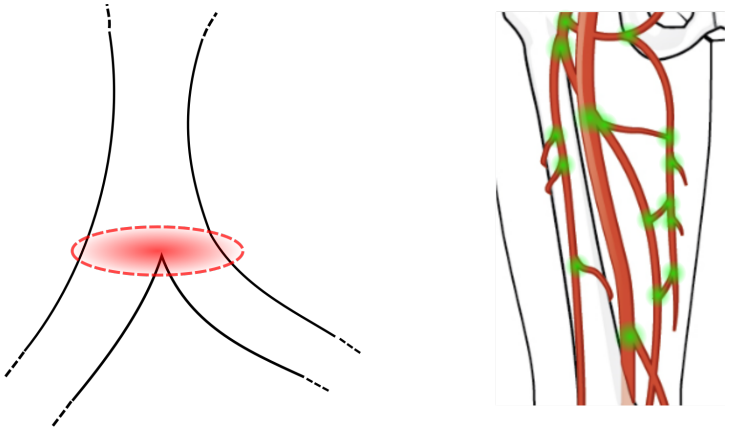

Figure 1: Left: A bifurcation location shown schematically in red oval, Right: Multiple bifurcation locations (highlighted in green) of a vascular system in a right leg. The right image was extracted from OpenStax College, Anatomy & Physiology [Ope14] and further modified. The book is available as a free download.

clear how the method would perform on a wider range of vascular landmarks. Besides, the algorithm is computationally demanding.

Zhou et al. [ZCMA07] proposed a method for vascular structure segmentation with an automatic method for bifurcation detection using AdaBoost classification on vessel cross-sectional images. The algorithm was evaluated on pulmonary vessels from clinical CT chest data. A success rate of 97% for bifurcation detection was reported.

A joint vessel tracking and bifurcation detection algorithm was introduced by Zhao et al. [ZH14]. The authors proposed three novel 3D features for classification by Random Forest. The algorithm was tested on 3D CT chest images as well as synthetic data. The performance of the algorithm was compared graphically with the method proposed by Zhou et al. [ZCMA07]. No numerical results were provided.

In contrast to other bifurcation detection methods, the algorithm proposed by Brozio et al. [BGG*12] as well as our approach do not need a complete segmentation of a vessel in 3D volume. The algorithm analyzes cross-sectional planes orthogonal to the vessels in a slicewise manner. To get the artery candidates, vessel candidates are obtained by thresholding and connected component analysis and further connected by using Dijkstra algorithm. A set of geometric features (such as shape and length) is used then to detect candidates for bifurcations. The algorithm was evaluated on abdomen and runoff contrast enhanced CT volumes. An overall bifurcation detection rate of 75.63% for iliac bifurcation was reported. Results for other vascular structures were not reported but authors claim that with minor changes the algorithm can be easily adapted.

Contribution In this work we present a real-time cascade classification algorithm for bifurcation detection in CTA images. We train two classifiers for two separate steps of the algorithm. The first classifier is trained to differentiate locations with a high concentration of bone structures next to the vessel, the second one to differentiate bifurcations. The algorithm does not require a full segmentation of the vessel tree to function properly. It can either be a part of a bigger vessel tracking algorithm and be able to classify bifurcation location on the fly or can be used to postprocess already existing vessel trees. The algorithm is fast, able to work in real-time and can be integrated into bigger vessel analysis systems. We demonstrate the performance of our algorithm on vessels from various parts of the body - head, neck and legs.

2. Materials and Methods

As the appearance of vessels varies greatly in different human body parts it is challenging to define a generic approach able to cope with all possible scenarios. In cross-sectional images vessels usually appear as bright structures on dark surrounding (see Figure 2a). In Figures 2b and 2c typical cross-sections of bifurcations are shown. In most cases bifurcations look like two smaller vessels merged together. Many arteries, such as vertebral, basilar and carotid ones, can differ in intensity as they pass through or run right next to bone structures (see Figure 2d). In those cases intensities of bone structures and vessels are similar and therefore there is no clear border visible between them. To the best of our knowledge and experience there are no large bifurcations in the vessel locations next to bone structures and therefore we propose to exclude those patches as the first step of the algorithm. At the second step we first segment the area within the vessel outer wall and then classify the shape of the segmented region.

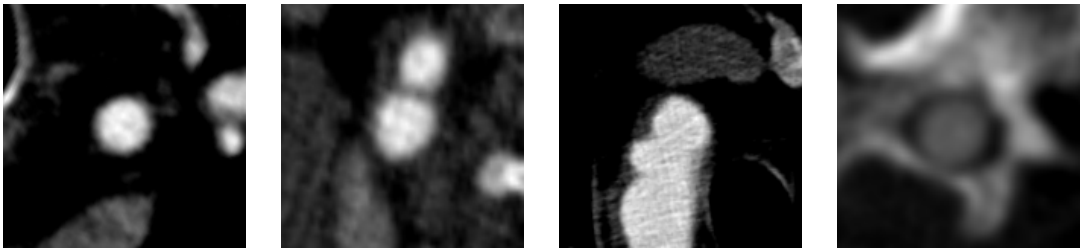

(a) (b) (c) (d)

Figure 2: Cross-sectional images of (a) a normal vessel, (b) a bifurcation, (c) a double bifurcation (d) vessel passing through a bone.

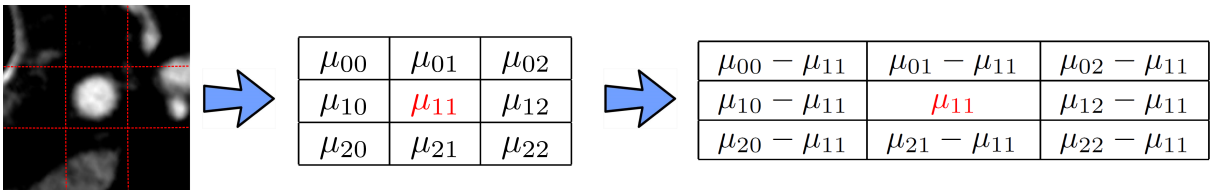

Figure 3: Feature generation for DDPI descriptors.

On each given candidate position the algorithm performs the following four steps:

1. Reconstruct a vessel-cross section (see Section 2.1).
2. Classify whether the vessel is located next to bone structures using combinations of features and classifiers explained in Sections 2.2 and 2.3 respectively.
3. Segment the interior area within vessel outer wall by a method explained in Section 2.4.
4. Classify whether the segmented shape represents a bifurcation using a set of boundary descriptors introduced in Section 2.5 and a classifier explained in detail in Section 2.3.

2.1. Vessel Cross-section Reconstruction

In order to generate a cross-section we need a point within a vessel wall and a tangential vector at the point. If a path within a vessel (e.g. a centerline of a vessel) is given the vector can be easily computed.

We use the method by Zambal et al. [ZHKB08] to extract vessel centerlines. Vessel cross-sections are computed then at the centerline points.

An image patch P^i with the center located at the given centerline point is extracted using trilinear interpolation - a value at each position of the patch is interpolated using intensity values at eight direct neighbouring voxels of the initial volume. As the size of a vessel is not known in advance the algorithm should be able to generate an image patch in a way that any possible human artery cross-section of a vessel bifurcation would fit into it. In our experiments the average size of a patch was approximately 10 mm with maximal size up to 40 mm for certain large arteries.

2.2. Feature representation for intensity-based cross-section classification

To train the algorithm to differentiate between the patches with clearly seen vessels from the patches with bone structures we evaluated several features which we briefly introduce below.

Histogram of Oriented Gradients (HOG) The descriptor thoroughly explained by Dalal et al. [DT05] counts occurrences of gradient information in localized portions of an image. The HOG features are widely used in medical image processing tasks. An excellent reference is given by Erdt et al. [EKDW13], where HOG features are applied to detect multiple anatomical regions simultaneously. For our problem, HOG features are of use in the first classification stage, because patches showing bone structures exhibit high local gradients in the bone as well as at the bone edges. Hence they are distinguishable from normal vessel patches, where high gradients occur mainly at the vessel borders.

Haralick Texture Features (HTF) Haralick et al. [HSD73] proposed a set of simple texture features based on gray-scale spatial dependencies applied to the image classification problem. HTF features have been actively used in medical image processing. Felipe et al. [FTTJ03] proposed a method which used the features for content retrieval from medical images for tissue identification and image classification. Another excellent example is the method proposed by Ghosh et

al. [GACD11] where the features were used for automatic diagnosis of lumbar intervertebral disc degeneration. In the original paper 14 descriptors were introduced. In our experiments we used ten: angular second moment, contrast, correlation, sum of squares (variance), inverse difference moment, sum average, sum variance, sum entropy, difference variance and difference entropy. Texture patches of bone and vessel samples vary in the spatial gray-scale relation and exhibit different contrasts, which makes it reasonable to evaluate HTFs for our method. Furthermore, they are simple and fast to compute. For more details on the features and implementation we refer to the original paper [HSD73].

Directional Derivatives of Pixel Intensities (DDPI) We propose a simple set of intensity-based features.

For each patch we repeat the following steps:

1. Subdivide the patch P^i into nine sub-patches P^i_{jk} (see Figure 3) where $j,k \in [0,2]$.

2. As the image patch is extracted in a way the center point is located within the vessel wall we assume that the central sub-patch lies partially or fully inside the vessel and therefore becomes a "reference" sub-patch.

3. For each sub-patch P^i_{jk}, compute the mean intensity μ_{jk} of its pixels.

4. Subtract the mean intensity of the reference sub-patch from mean intensities of the other sub-patches.

5. Form an eight-dimensional feature vector

$$v_k = (\mu_{00} - \mu_{11},\ \mu_{01} - \mu_{11}, \ldots,\ \mu_{22} - \mu_{11})^T \quad (1)$$

6. Make the feature rotation invariant by sorting the values of each vector v_k in ascending order.

7. Train the classier with feature vectors Eq. 1 for two classes - normal case without bones located next to the vessel (including cases with bifurcations), and the case when the vessel is passing through or running close to bone structures.

Feature visualization The t-Distributed Stochastic Neighbor Embedding (t-SNE) (Van et al. [VdMH08]) representation of the three features is depicted in Figure 4. As you can see from the figures all three features demonstrate reasonable separability for our problem and can be applied to separate bone cases (shown in red) from normal vessel locations (shown in blue).

2.3. Classification Algorithms

For our problem we used two supervised learning classification algorithms.

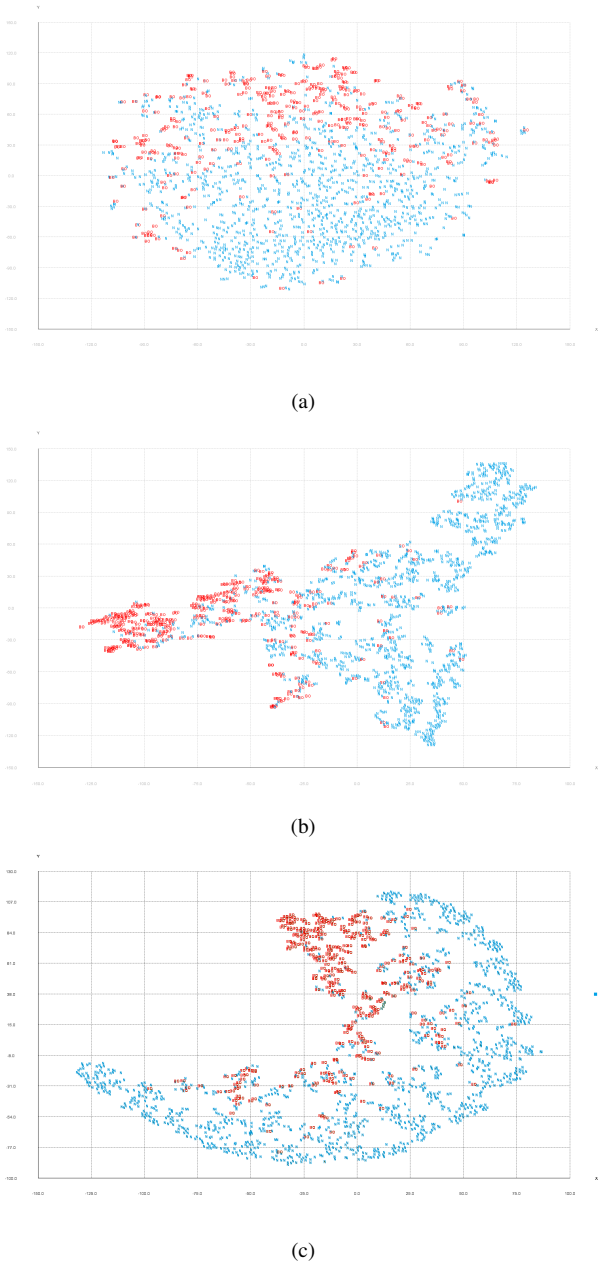

(a) (b) (c)

Figure 4: t-SNE visualizations of (a) HOG, (b) HTF, (c) DDPI features; horizontal and vertical axes represent t-SNE values estimated from the corresponding features.

The Approximate Nearest Neighbour Method (ANN) Priority Search K-Means algorithm proposed by Muja et al. [ML14] belongs to a class of approximate nearest neighbour algorithms and is extremely efficient especially when either the feature space dimension or the number of training samples is large. The search tree is constructed by separat-

ing points at each tree level into M distinct regions using k-means clustering until the number of points in the region is smaller than M.

The Support Vector Machine (SVM) algorithm introduced by Vapnik and Chervonenkis [VC64] and in current standard incarnation proposed by Cortes and Vapnik [CV95], efficiently performs a non-linear classification by constructing a hyperplane which would represent the largest separation between the classes. SVM proved its oustanding efficiency when working with HOG features in image processing particularly (see Bristow and Lucey [BL14] for a nice explanation why).

At the first level of the scheme we compared both classifiers - ANN and SVM in combination with three different features. In the second part of the scheme only the ANN on boundary features has been used.

2.4. Morphological Active Contour Without Edges (MACWE) for Vessel Outer Wall Segmentation

The basis for the segmentation algorithm is the approximation of the model proposed by Chan et al. [CSV00].

The proposed method was designed for detecting objects where boundaries are not necessarily defined by gradient information. The active contour without edges functional of a curve C is defined as:

$$F(c_1,c_2;C) = \mu\,\text{Length(C)} + \nu\,\text{Area(inside(C))} + \lambda_1 \int_{inside(C)} \| I(x) - c_1 \|\, dx\, dy + \lambda_2 \int_{outside(C)} \| I(x) - c_2 \|\, dx\, dy \quad (2)$$

where $\mu \geq 0, \nu \geq 0, \lambda_1, \lambda_2 > 0$ are fixed parameters, c_1 and c_2 are the mean of the values of $I(x)$ inside and outside the contour C.

We consider the minimization problem:

$$\inf_{c_1,c_2,C} F(c_1,c_2,C) \quad (3)$$

As an initial object for the algorithm, we used a small circle with the center at the given starting point.

We use the morphological approximation for the problem in Eq. 3 (introduced by Alvarez et al. [ABHMN10]) because it does not require solving a numerical PDE unlike the original model and therefore does not suffer from numerical stability problems. Besides, morphological operators are easier and more straightforward to implement than complicated numerical algorithms.

2.5. Feature representation for segmented shape classification

For classification of the segmented object we use some of the boundary descriptors nicely summarized in the thesis by Huque [Huq06]. In order to compute the descriptors we outline the segmentation first by using morphological operators (dilation followed by subtraction) and then fit the minimum-bounding rectangle to the outline using the method proposed by Chaudhuri et al. [CS07].

The following descriptors we find suitable for our problem i.e. they are capable of differentiating between circular and elliptic shapes (shapes which vessels and bifurcations normally have) or highly concave shapes which in turn could result from a failed segmentation.

Elongation (by Jenkin et al. [HJ97]) :

$$\text{Elongation} = \frac{\text{width}_{\text{bounding-box}}}{\text{height}_{\text{bounding-box}}} \quad (4)$$

Eccentricity (by Gonzalez and Woods [GW01]) :

$$\text{Eccentricity} = \frac{\text{axis length}_{\text{short}}}{\text{axis length}_{\text{long}}} \quad (5)$$

Convexity (by Shipley and Kellman [SK01]) :

$$\text{Convexity} = \frac{\text{convex perimeter}}{\text{perimeter}} \quad (6)$$

Solidity (by Derry [Der02]):

$$\text{Solidity} = \frac{\text{area}}{\text{convex area}} \quad (7)$$

Standard Deviation of Radial Distances:

$$S_d = \sqrt{\frac{1}{N-1} \sum_{i=1}^{N} (\, d_i - \overline{d}\,)^2} \quad (8)$$

where $i \in [1,N]$; d_i is the radial distance, i.e. the distance from the center of mass to the perimeter point $(x_i,\ y_i)$.

3. Evaluations

3.1. Data

To evaluate our approach we used the following datasets:

- Seven head & neck CTA scans with dimensions 512×512, number of slices from 754 to 1001, in-plane sizes $(0.32-0.43) \times (0.32-0.43)$ mm^2, and slice thickness 0.3 mm for all scans.
- Three leg CTA scans with dimensions 512×512, number of slices from 704 to 1084, in-plane sizes 0.67×0.67 mm^2, and slice thickness from 1.0 to 1.5 mm.

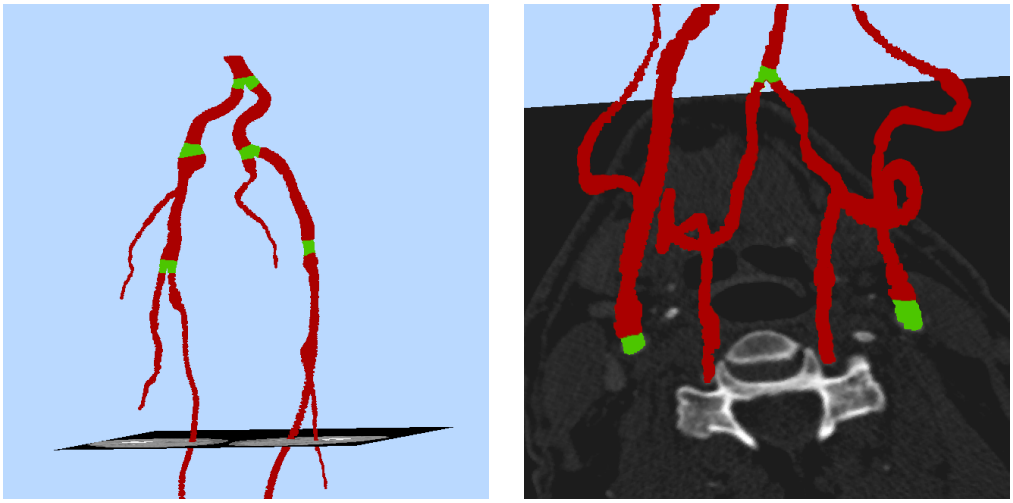

(a) (b)

Figure 5: Two cases of vessel trees and bifurcation locations for (a) a leg study, (b) a head & neck study.

3.2. Reference Data

Vessel centerlines for all datasets were annotated by a medical expert. Each position in the centerline was labeled as a bifurcation, normal position or a position with a large concentration of bone structures next to the vessel.

3.3. Evaluation metrics

For the evaluations we used the following performance metrics:

Success Rate (SR):

$$\text{SR} = \frac{\text{TP}+\text{TN}}{\text{TP}+\text{TN}+\text{FP}+\text{FN}} \times 100\% \qquad (9)$$

Failed Rate (FR):

$$\text{FR} = \frac{\text{FP}}{\text{TP}+\text{TN}+\text{FP}+\text{FN}} \times 100\% \qquad (10)$$

Missed Rate (MsR):

$$\text{MsR} = \frac{\text{FN}}{\text{TP}+\text{TN}+\text{FP}+\text{FN}} \times 100\% \qquad (11)$$

3.4. Results

For all tests we used patches with dimensions 160×160 pixels. We performed cross-validations for seven head & neck and three leg datasets. In total more than 3500 cross-sectional images of 34 vessels from various parts of the human body have been examined.

Intensity-based cross-section classification The main aim of the first part of the algorithm was excluding as many "bone samples" as possible and at the same time keeping samples with bifurcations.

Measures	# 1	# 2	# 3
SR (%)	88.76	87.54	85.43
FR (%)	3.64	4.46	4.8
MsR (%)	7.6	8.0	9.7

Table 1: Leave-one-out cross-validation results of the first step of the algorithm for head & neck datasets for three intensity-based classification pairs - #1: HOG + SVM, #2: HTF + SVM, #3: DDPI + ANN.

Measures	#1+ANN	#2+ANN	#3+ANN
SR (%)	86.74	87.66	83.64
FR (%)	8.79	7.14	11.99
MsR (%)	4.4	5.19	4.36

Table 2: Final results after two steps of the pipeline algorithm for head & neck datasets for three configurations of intensity-based classification pairs at the first step and boundary descriptors with ANN at the second step.

Cross-validation results for the best configurations for all three features for head & neck datasets are shown in Table 1.

For the leg datasets there were very few cases with bone structures next to the vessel and therefore the success rate was about 96-98 % for all three configurations. Overall numbers shown in Table 1 demonstrate that HOG and HTF in combination with SVM outperform DDPI with ANN but at the same they require more feature and parameter tuning. For the generation of the symmetric gray-level co-occurrence matrix for HTFs, grid search was performed on various distance and angle settings. Best results were achieved with a distance of one, i.e. using the direct neighbour, and an an-

Measures	Circle of Willis	Middle Cerebral	Subclavian	Vertebral	Carotid	Brachiocephalic Trunk	Cerebellar*	Overall Result
SR (%)	83.33	93.93	78.65	82.29	79.52	96.29	94.23	84.37
FR (%)	6.8	1.51	15.85	12.11	12.9	0.0	3.84	11.25
MsR (%)	9.8	4.54	5.48	5.59	7.56	3.7	1.92	4.37

Table 3: Head & neck study results for the bifurcation detection for the best performing HTF and SVM configuration; (*) corresponds to left and right anterior inferior cerebellar and left and right superior cerebellar arteries.

Measures	Aorta	Iliac Arteries	Femoral Arteries	Peroneal Arteries	Overall Result
SR (%)	100.0	86.36	92.68	82.4	87.68
FR (%)	0	13.22	2.43	12.4	8.79
MsR (%)	0	0.4	4.87	5.2	3.51

Table 4: Leg study results for the bifurcation detection for the best performing HTF and SVM configuration.

gle of 135 degrees. DDPI and ANN are both efficiently fast, show competitive results and can be used right out of the box in real-time applications.

Segmented shape classification At the second step of the algorithm, we classify bifurcation locations by analyzing geometric descriptors of the segmented shapes.

The algorithm segments the object of interest by MACWE with standard parameters ($\lambda_1 = 1$, $\lambda_2 = 1$, $\mu_1 = 1$) and then computes five boundary descriptors introduced in Section 3.4. ANN with branching factor $M = 16$ and $K = 15$ neighbours is used to classify the segmented shape. Both parameter sets have been recommended in the original papers by Neila et al. [MNBA14] and Muja et al. [ML14].

Table 2 shows the results after the second step of the classification algorithm for all three configurations used at the first step. Final results demonstrate that successful classification rate of the segmented shapes for samples preselected by the combination of HTF with SVM slightly exceeds the other configurations used at the first step of the cascade algorithm.

Tables 3 and 4 show detailed cross-validation results for particular arteries in head & neck and leg studies respectively for the best performing combination of the intensity-based classification pair HTF + SVM configuration together with ANN algorithm for segmented shape classification task. Relatively high failed rate for subclavian, vertebral and carotid (internal carotid particularly) arteries is caused by a high concentration of bone structures close to the arteries. Accordingly small glitches in the segmentation algorithm in those cases led to undesirable misclassifications.

Figure 5 shows resulting vessel trees for two datasets with bifurcation locations highlighted in green color.

Our algorithm shows better overall results for carotid arteries than the result claimed by Beck et al. [BBBD10] for left and right carotid bifurcations - 79.52 % against 74.47 % and 78.72 % respectively. Compared to Brozio et al. [BGG*12], whose algorithm is also working with cross-sectional images, our method demonstrated higher overall bifurcation detection success rate for iliac artery bifurcations - 86.36 % against 75.63 % reported by the authors. Besides that, our evaluations include not only the main iliac artery bifurcation, but also other smaller bifurcations of the iliac arteries. The overall results with success rates of 84.37 % for head & neck and 87.68 % for leg studies demonstrate that our algorithm is competitive with other state-of-the art methods. Besides, in contrast to other methods our algorithm can deal with various arteries and even small bifurcations in different parts of the human body.

Algorithm performance All evaluations have been performed on a PC with 16 GB RAM with a 3.40 GHz Intel Xeon CPU within a single-threaded framework. Total processing time for 3500 cross-sectional images was 275 s with an average processing time of 0.08 s per testing sample.

4. Conclusions

We presented a two-level algorithm for artery bifurcation detection in different parts of a human body in CTA images. Our approach is straight-forward to implement: we use classic and simple features for classification, an easy-to-tune algorithm for segmentation of the vessel outer wall and further classification of the segmented shape. Our method shows encouraging and competitive results on various arteries in head, neck and leg datasets. We believe our algorithm can be applied to vessels in other parts of a human body. As the algorithm does not use any CTA-specific information it can be easily adopted to blood vessel images from other imaging modalities. Timing measures show that the algorithm is suitable for bigger real-time vessel analysis systems. We believe that our results can even be improved with more training data and a learning-based segmentation algorithm. As future work we plan to extend the algorithm to 3D, i.e. we

believe it will improve robustness of the whole method in problematic cases.

Acknowledgements

The competence center VRVis with the grant number 843272 is funded by BMVIT, BMWFW, and the Vienna Business Agency within the scope of COMET – Competence Centers for Excellent Technologies. The program COMET is managed by FFG. Thanks go to our project partner AGFA Healthcare for providing data and valuable input.

References

[ABG*12] ALBERTI M., BALOCCO S., GATTA C., CIOMPI F., PUJOL O., SILVA J., CARRILLO X., RADEVA P.: Automatic bifurcation detection in coronary ivus sequences. *Biomedical Engineering, IEEE Transactions on 59*, 4 (2012), 1022–1031. 1

[ABHMN10] ALVAREZ L., BAUMELA L., HENRIQUEZ P., MARQUEZ-NEILA P.: Morphological snakes. In *Computer Vision and Pattern Recognition (CVPR), 2010 IEEE Conference on* (June 2010), pp. 2197–2202. doi:10.1109/CVPR.2010.5539900. 5

[BBBD10] BECK T., BERNHARDT D., BIERMANN C., DILLMANN R.: Validation and detection of vessel landmarks by using anatomical knowledge. In *SPIE Medical Imaging* (2010), International Society for Optics and Photonics, pp. 76234I–76234I. 1, 7

[BGG*12] BROZIO M., GORBUNOVA V., GODENSCHWAGER C., BECK T., BERNHARDT D.: Fast automatic algorithm for bifurcation detection in vascular cta scans, 2012. URL: http://dx.doi.org/10.1117/12.911329, doi:10.1117/12.911329. 2, 7

[BH12] BABOIU D., HAMARNEH G.: Vascular bifurcation detection in scale-space. In *Mathematical Methods in Biomedical Image Analysis (MMBIA), 2012 IEEE Workshop on* (Jan 2012), pp. 41–46. 1

[BL14] BRISTOW H., LUCEY S.: Why do linear svms trained on hog features perform so well? *arXiv preprint arXiv:1406.2419* (2014). 5

[CS07] CHAUDHURI D., SAMAL A.: A simple method for fitting of bounding rectangle to closed regions. *Pattern Recogn. 40*, 7 (July 2007), 1981–1989. URL: http://dx.doi.org/10.1016/j.patcog.2006.08.003, doi:10.1016/j.patcog.2006.08.003. 5

[CSV00] CHAN T. F., SANDBERG B., VESE L. A.: Active contours without edges for vector-valued images. *Journal of Visual Communication and Image Representation 11*, 2 (2000), 130 – 141. URL: http://www.sciencedirect.com/science/article/pii/S104732039990442X, doi:http://dx.doi.org/10.1006/jvci.1999.0442. 5

[CV95] CORTES C., VAPNIK V.: Support-vector networks. *Machine learning 20*, 3 (1995), 273–297. 5

[Der02] DERRY G. N.: *What science is and how it works*. Princeton University Press, 2002. 5

[DT05] DALAL N., TRIGGS B.: Histograms of oriented gradients for human detection. In *Computer Vision and Pattern Recognition, 2005. CVPR 2005. IEEE Computer Society Conference on* (June 2005), vol. 1, pp. 886–893 vol. 1. doi:10.1109/CVPR.2005.177. 3

[EKDW13] ERDT M., KNAPP O., DRECHSLER K., WESARG S.: Region detection in medical images using hog classifiers and a body landmark network, 2013. URL: http://dx.doi.org/10.1117/12.2007384, doi:10.1117/12.2007384. 3

[FTTJ03] FELIPE J. C., TRAINA A. J., TRAINA JR C.: Retrieval by content of medical images using texture for tissue identification. In *Computer-Based Medical Systems, 2003. Proceedings. 16th IEEE Symposium* (2003), IEEE, pp. 175–180. 3

[GACD11] GHOSH S., ALOMARI R., CHAUDHARY V., DHILLON G.: Computer-aided diagnosis for lumbar mri using heterogeneous classifiers. In *Biomedical Imaging: From Nano to Macro, 2011 IEEE International Symposium on* (2011), IEEE, pp. 1179–1182. 4

[GW01] GONZALEZ R. C., WOODS R. E.: *Digital Image Processing*, 2nd ed. Addison-Wesley Longman Publishing Co., Inc., Boston, MA, USA, 2001. 5

[HJ97] HARRIS LAURENCE (LAURENCE ROY) ., JENKIN MICHAEL (MICHAEL RICHARD MACLEAN) .: Computational and psychophysical mechanisms of visual coding, 1997. Based on a conference on visual coding, 3rd conference of the York Center for Vision Research, in June 1995. 5

[HSD73] HARALICK R., SHANMUGAM K., DINSTEIN I.: Texture features for image classification. *IEEE Transactions on Systems, Man, and Cybernetics 3*, 6 (1973). 3, 4

[Huq06] HUQUE A.: *Shape analysis and measurement for the HeLa cell classification of cultured cells in high throughput screening*. School of humanities and informatics. Högskolan, 2006. URL: https://books.google.at/books?id=89cdnwEACAAJ. 5

[ML14] MUJA M., LOWE D.: Scalable nearest neighbor algorithms for high dimensional data. *Pattern Analysis and Machine Intelligence, IEEE Transactions on 36*, 11 (Nov 2014), 2227–2240. 4, 7

[MNBA14] MARQUEZ-NEILA P., BAUMELA L., ALVAREZ L.: A morphological approach to curvature-based evolution of curves and surfaces. *IEEE Transactions on Pattern Analysis and Machine Intelligence 36*, 1 (2014), 2–17. doi:http://doi.ieeecomputersociety.org/10.1109/TPAMI.2013.106. 7

[Ope14] OPENSTAX: *Anatomy & Physiology*. OpenStax CNX, Nov 7 2014. URL: http://cnx.org/contents/14fb4ad7-39a1-4eee-ab6e-3ef2482e3e22@7.16. 2

[SK01] SHIPLEY T. F., KELLMAN P. J.: *From fragments to objects: Segmentation and grouping in vision*, vol. 130. Elsevier, 2001. 5

[VC64] VAPNIK V., CHERVONENKIS A.: A note on one class of perceptrons. *Automation and remote control 25*, 1 (1964). 5

[VdMH08] VAN DER MAATEN L., HINTON G.: Visualizing data using t-sne. *Journal of Machine Learning Research 9*, 2579-2605 (2008), 85. 4

[ZCMA07] ZHOU J., CHANG S., METAXAS D., AXEL L.: Vascular structure segmentation and bifurcation detection. In *Biomedical Imaging: From Nano to Macro, 2007. ISBI 2007. 4th IEEE International Symposium on* (2007), IEEE, pp. 872–875. 2

[ZH14] ZHAO M., HAMARNEH G.: Bifurcation detection in 3d vascular images using novel features and random forest. In *Biomedical Imaging (ISBI), 2014 IEEE 11th International Symposium on* (April 2014), pp. 421–424. 2

[ZHKB08] ZAMBAL S., HLADUVKA J., KANITSAR A., BUEHLER K.: Shape and appearance models for automatic coronary artery tracking. 3